PERGAMON

Electrochimica Acta 44 (1999) 1697–1705

ELECTROCHIMICA Acta

# Molecular simulation of the electrochemical double layer

E. Spohr[1]

*Department of Theoretical Chemistry, University of Ulm, Albert-Einstein-Allee 11, 89069 Ulm, Germany*

Received 23 February 1998

**Abstract**

Direct computer simulations of the electrochemical double layer between an aqueous electrolyte solution and a metal surface have recently become possible, although currently only at high electrolyte concentrations. In the present study molecular dynamics simulations of the structure of a 2.2 molal aqueous NaCl solution in the vicinity of an idealized metal surface are reported. Uncharged as well as positively and negatively charged metal surfaces are investigated. 

*Keywords:* Electrochemical double layer; Molecular dynamics; Molecular simulation; Ion distribution; Ion adsorption

## 1. Introduction

The field of computer simulations of electrochemical systems has grown into a very active branch of modern physical and theoretical chemistry (for some recent reviews, see, for example, Refs. [1–5]). Contrary, and complementary, to most experimental and higher-level quantum mechanical techniques, molecular simulations can realistically model the role of the solvent, which is usually by far the most abundant species near the electrochemical interface. The molecular nature of the solvent manifests itself for instance in density oscillations near the interface due to packing effects and in ion solvation.

In classical models of the electrochemical double layer, like the Helmholtz [6], Gouy-Chapman [7, 8] and Stern [9] double layer models the solvent is either neglected altogether or enters summarily in the form of its dielectric constant. More advanced models like the one by Parsons [10] incorporate the adsorbed water layer by means of an excluded volume and the reduced orientational mobility in the interfacial region in the form of a distance-dependent dielectric constant. None of the above models incorporates the inhomogeneity of the charge distribution in the interfacial region and the finite size and shape anisotropy of molecules or ions.

For a long time interaction site models have been used successfully in computer simulations of bulk aqueous solutions to study the structure and dynamics of simple electrolyte solutions. Interaction site models of water usually consist of three charged sites, representing the oxygen and the two hydrogen atoms. Many different parametrizations exist in the literature, but all of them are to some extent able to describe the phenomenon of hydrogen bonding between water molecules and the hydration of simple ions dissolved in water. Application of interaction site models to a two-phase aqueous/metallic system creates a realistic microscopic model of the double layer, at least in the absence of electrochemical reactions. Such a model allows us to investigate the validity and limits of electrochemical concepts developed on the basis of the older models.

In the present study, interaction site models for water and $Na^+$ and $Cl^-$ are employed to simulate the double layer between a 2.2 molal NaCl solution and a simple model of a metallic phase. Specifically, changes in the so-called diffuse and contact layers are investigated when changing the surface charge on the 'metal electrode' from negative through neutral to positive values, as in a typical electrochemical experiment. The analysis follows in part that by Philpott and

[1] E-mail: eckhard.spohr@chemie.uni-ulm.de

0013-4686/99/$ - see front matter 
PII: S0013-4686(98)00289-8

Glosli [4, 11, 12], who studied the concentration dependence of the double layer properties of aqueous NaCl in contact with a negatively charged electrode, using a similar model with slightly different potential parameters (see below). Contrary to their study and the present one, other simulations of concentrated electrolyte solutions near interfaces [13–16] did not have sufficient statistical accuracy to reliably predict ion distributions near the interface.

The layout of the paper is as follows: in Section 2 I will discuss the microscopic models and the methods employed. Then, in Section 3 the structure of the double layer region is investigated, and questions pertaining to the thickness of the double layer and the validity of the Gouy-Chapman theory are addressed. The results are compared to the work of Philpott and Glosli. In Section 4, the results will be related to simple electrochemical concepts.

## 2. Models and methods

In the present study the interface of a 2.2 molal aqueous NaCl solution in contact with a simple model of the metal is modeled. The aqueous phase is a thin liquid film which forms on one side the interface to the metal phase and on the other side a free liquid/vapor interface. Water is described by the rigid SPC/E model [17]. This model consists of three point charges of $-0.8476e$ on the oxygen and $0.4238e$ on the hydrogen atom sites. $e$ is the proton charge. Dispersion interactions and short range repulsion is accounted for by representing the oxygen atom as a Lennard–Jones sphere. Ions are modeled as charged Lennard–Jones spheres. The Lennard–Jones parameters for ion–ion and ion–water interactions are taken from the work of Bopp et al. [18] and Dang and Smith [19, 20] (see also Ref. [21]), respectively. They are summarized in Table 1.

A simple external potential that incorporates the effect of surface corrugation and anisotropic adsorption was used to model the metal surface [22]. The water–metal potential consists of a Morse function, augmented by a corrugation term for oxygen–surface and a repulsive term for hydrogen–surface interactions:

$$V_{\text{water–surface}} = \phi_{\text{O}}(x_{\text{O}}, y_{\text{O}}, z_{\text{O}}) + \phi_{\text{H}}(z_{\text{H1}}) + \phi_{\text{H}}(z_{\text{H2}}) \quad (1)$$

with

$$\phi_{\text{O}}(x, y, z) = 12[\exp(-2(z-3)) - 2\cdot\exp(-(z-3))] + 3\exp(-2(z-3)) \times \left[\cos\left(\frac{10\pi x}{L_x}\right) + \cos\left(\frac{10\pi y}{L_y}\right)\right] \quad (2)$$

and

$$\phi_{\text{H}}(x, y, z) = 24\exp(-2(z+1)). \quad (3)$$

Energies are in kJ $\text{mol}^{-1}$ when distances are given in Å. The corrugation is felt only in the repulsive part of the Morse potential function and has a periodicity of 3.6 Å in both directions parallel to the surface, corresponding to a (100) surface with a nearest neighbour distance of 2.55 Å. Since the hydrogen–surface interactions are weakly repulsive, binding occurs predominantly through the oxygen atoms. This is in keeping with available experimental and theoretical evidence [23]. Anions and cations interact with the surface by means of the same interaction potential as the oxygen atoms.

The metallic nature of the interface is modelled by the image charge model. The static image plane is located at $z = 0$ Å. Each partial charge in the system interacts with the complete set of real charges and image charges. Through the incorporation of the image charges the total system remains uncharged even if a different number of real cations and anions is dissolved in the aqueous phase (see below). Long-range corrections for the Coulomb interactions are taken into account by a tabulated version of the Ewald sum for systems with slab boundary conditions (i.e. systems which are periodic in two dimensions and of finite extent in the third one). Appropriate long-range corrections are mandatory for simulations of the kind reported here. It was recently demonstrated [24–26] that truncation schemes lead to unphysical electric fields in the center of a slab that preclude the formation of a 'bulk' region in the simulation.

All simulated systems consist of 400 water molecules and 32 ions in a tetragonal unit cell with box sizes $L_x = L_y = 18$ and $L_z = 200$ Å. Periodic boundary conditions are employed in the two directions parallel to the interface. If there is an excess of cations or anions, the liquid side of the interface carries a net charge. The net image charge is the negative of this charge and corresponds in the present model to the surface charge.

Table 1. Lennard–Jones parameters ($V_{\text{LJ}} = 4\epsilon[(\sigma/r)^{12} - (\sigma/r)^{6}]$)

| | $\epsilon$ ($10^{-23}$ J) | $\sigma$ (Å) |
|---|---|---|
| O–O | 107.95 | 3.169 |
| O–$Na^+$ | 86.60 | 2.876 |
| O–$Cl^-$ | 86.60 | 3.250 |
| $Na^+$–$Na^+$ | 59.37 | 2.73 |
| $Na^+$–$Cl^-$ | 28.32 | 3.87 |
| $Cl^-$–$Cl^-$ | 27.87 | 4.86 |

Three different systems are simulated: one with an equal number of cations and anions ($16Na^+ + 16Cl^-$) and an uncharged metal surface and two simulations with positive ($+2e$, $15Na^+ + 17Cl^-$) and negative surface charges ($-2e$, $17Na^+ + 15Cl^-$) The chosen boundary conditions imply the control of the surface charge rather than the usual experimental situation of potential control. The potential change can be calculated from the solution of the one-dimensional Poisson equation. The simulations thus correspond to the situation at the potential of zero charge and surface charge densities of $+9.9$ μC $cm^{-2}$ and $-9.9$ μC $cm^{-2}$.

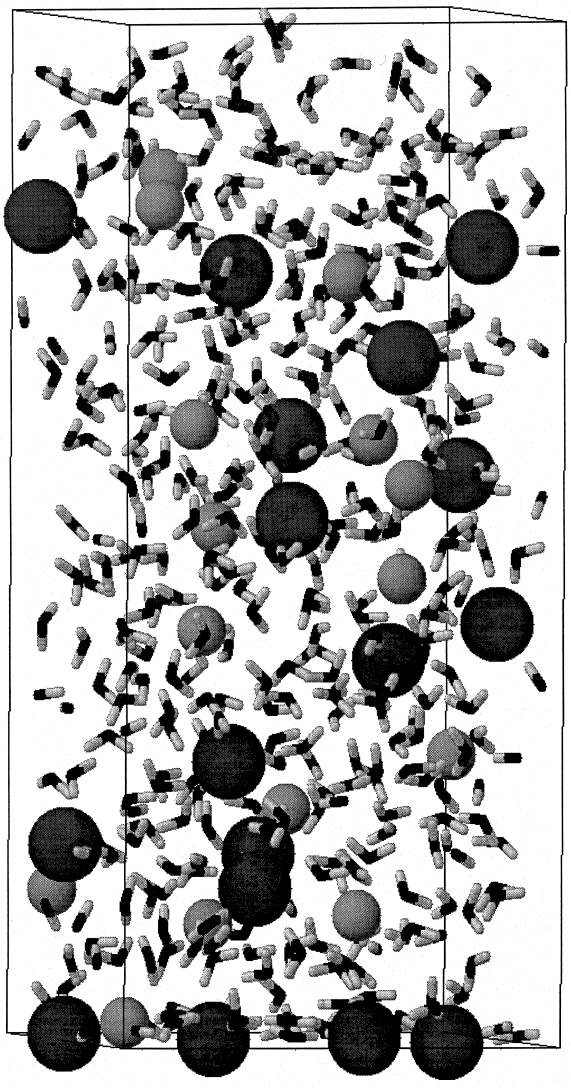

Fig. 1. Snapshot of the simulation with surface charge $\sigma = +9.9$ μC $cm^{-2}$. $Na^+$: small spheres, $Cl^-$: large spheres. The liquid slab is confined by the metal surface (bottom) and by a 'free' surface (top).

Molecular dynamics (MD) simulations were performed for these systems with an integration time step of 2.5 fs for 2.2 ns after an extensive equilibration period of 100 ps. The SHAKE constraint algorithm and the VERLET algorithm [27], have been used to integrate the equations of motion. The temperature was kept constant at 298.15 K by coupling to a Berendsen thermostat [28] with time constant 0.4 ps. The long simulation time is necessary in order to obtain statistically converged results for the ion distributions, since the double layer is not a rigid entity like, for example, in the Helmholtz model but very inhomogeneous both in space and in time.

Fig. 1 shows a snapshot of the simulation cell for surface charge $\sigma = +9.9$ μC $cm^{-2}$. The $z$-direction is from bottom to top and the metal phase is below the depicted cell. The large dark spheres are the $Cl^-$ ions, the small grey ones the $Na^+$ ions. In this particular configuration, four anions and one cation are adsorbed on the metal surface. It is also evident that the free surface (top) is depleted of ions.

## 3. Results

### 3.1. Density profiles

The most important structural quantities, which characterize the double layer on the molecular level, are the atom and ion density profiles. The density profiles are the ratio between the local density of a species at the interface and the bulk density of that species. Fig. 2 shows the oxygen and ion density profiles as a function of the distance $z$ from the metal surface at vanishing surface charge. The functions are obtained by averaging each local density over the two directions parallel to the interface and over the entire simulation time of 2.2 ns. The oxygen density profiles (dashed lines in Fig. 2) are mostly unchanged from those of pure water, when the same interaction parameters with the metal surface are used [22] and are given for comparison only.

While the oxygen density profiles are smooth and well converged, the ion density profiles are rather noisy, in spite of the fact that the simulation extends over a time longer than 2 ns. The noise level is due to the fact that even at the high electrolyte concentration the number of ions (16 cations and 16 anions) in the simulation cell is still rather small. Nevertheless, several key properties of the ion density profiles can be recognized that are not affected strongly by statistical uncertainties.

- The ionic densities near the liquid/gas interface decrease to a value of one half of the bulk density at approximately 3 Å from the corresponding value for

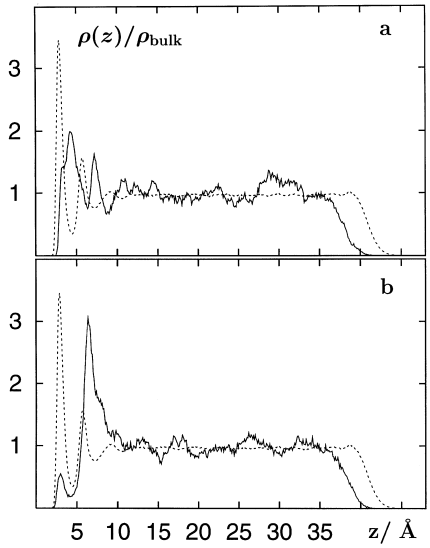


Fig. 2. Density profiles for the simulation with surface charge $\sigma = 0$. Top: cation (full line) and oxygen (dashed); bottom: anion (full line) and oxygen (dashed). Density profiles are normalized to the corresponding values of the bulk densities in a 2.2 molal NaCl solution.

the water density, which is indicative of a tendency to form at least one full hydration shell. The results are consistent with simulations by other authors [29–31] which showed that the water/gas interface is depleted of ions.

- In the vicinity of the metal surface the ionic densities are not monotonic, as might be expected on the basis of a simple extrapolation of the Gouy-Chapman theory to high concentrations. Rather, the ionic densities oscillate in the region $z < 10$ Å. The ion densities follow to some extent the oscillations of the oxygen density which are the consequence of the generic 'layering effect' occurring in liquids near a surface.
- The $Na^+$ density clearly shows two maxima which coincide with the local minima of the oxygen density profiles between first and second and the one between second and third layer. The arrangements lead, apparently, to an optimal formation of hydration complexes (see below).
- The $Cl^-$ density possesses a well-pronounced maximum at 7 Å, slightly beyond the second maximum of the oxygen density. The height of the anion maximum is significantly higher than the height of the corresponding maxima of the cations, indicating that the plane of negative charge is defined more sharply. In addition, a small maximum at contact with the metal surface is clearly visible for the $Cl^-$ profile.
- The oscillations of the ion density beyond $z \approx 10$ Å appear not to have a physical origin. The magnitude of the oscillations decreased during the simulation roughly proportional to the square root of the simulation time, which is indicative of a statistical effect due to finite simulation time and particle numbers. However, from the present work the persistence of small-amplitude oscillations beyond distances of 10 Å cannot be entirely ruled out.

Fig. 3 shows the ion density profiles near the metal surface for all three surface charges investigated here. Beyond $z = 20$ Å all ion density profiles are identical within the limits of statistical error. The oxygen density profile does not change much with surface charge and is repeated here only to provide a reference for the interpretation of ion densities. Together with the ion densities, $\rho(z)$, the running integrals of the densities, $n(z)$, defined by

$$n(z) = L_x L_y \int_0^z \rho(z')\,\mathrm{d}z', \tag{4}$$

are plotted for $Na^+$ (full lines) and $Cl^-$ (dashed lines). $L_x = L_y = 18$ Å are the box dimensions parallel to the interface and $\rho$ is the particle number density. The following observations are made:

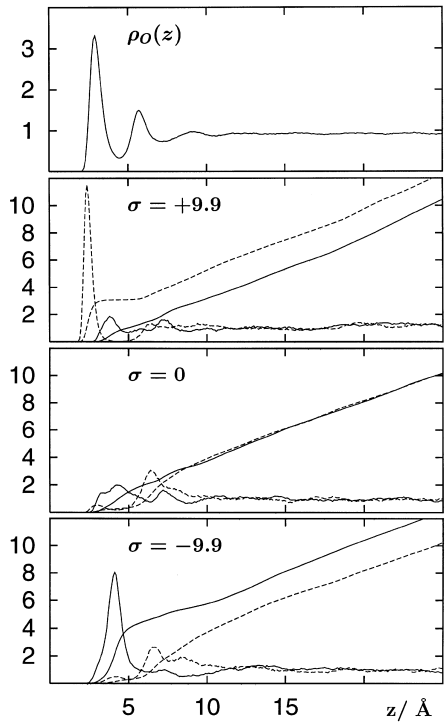


Fig. 3. Density profiles and running integrals $n(z)$ of the ion densities for $Na^+$ (full lines) and $Cl^-$ (dashed lines) at three different surface charge densities as indicated. The top frame contains the oxygen atom density profile of Fig. 2.

- At finite positive and negative surface charge densities, the counterion density profiles exhibit significantly higher maxima; the counterion positions are correlated more strongly with the charged metal surfaces than with the uncharged surface. This makes possible the definition of planes in which most of the countercharge is included, in analogy to the inner and outer Helmholtz planes of the classical electrochemical models.
- At the large positive surface charge ($\sigma = 9.9$ μC cm$^{-2}$) the chloride ions are attracted directly to the surface. From the running integral it can be concluded that about three $Cl^-$ ions are adsorbed on the surface. The three ions overcompensate the surface charge density which corresponds to only two elementary charges for the entire simulation cell. This behavior is in analogy with the concept of super-equivalent adsorption [32]. Approximately one cation remains in the interlayer region between the adsorbate water and the second layer. Hence, the surface charge of $2e$ is compensated by $\approx -3e$ from the anion density and $\approx +e$ from the cation density.
- At the negative surface charge ($\sigma = -9.9$ μC cm$^{-2}$) the maximum of the $Na^+$ density profile grows substantially but remains more or less at the same position as for the uncharged surface. At the same time the maximum of the anion density is shifted to the region between 6 and 9 Å. About 4 $Na^+$ ions are located in the region of this density maximum.
- In all cases, the density oscillations extend to a distance of about 10–12 Å.

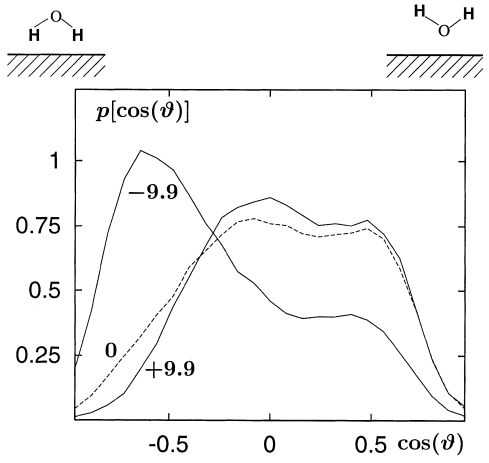


Fig. 4. Orientational distribution of the water dipole moment in the adsorbate layer of three simulations with different surface charge densities (in units of μC cm$^{-2}$ as indicated). cos $\vartheta$ is the angle between the water dipole vector and the surface normal that points into the aqueous phase.

- When the difference between the running integral of cations and anions becomes equal to the negative surface charge, the entire surface charge can be regarded as screened by the mobile charges. The distance at which this happens changes from about 5.5 Å ($\sigma = +9.9$ μC cm$^{-2}$) to about 8 Å ($\sigma = 0$) and 10 Å ($\sigma = -9.9$ μC cm$^{-2}$). Hence, the double layer thickness is to some extent dependent on the surface charge density. However, because of the limited statistical accuracy of the density profiles, some details may change upon further increase of simulation time. In all cases, the thickness of the double layer is of the order of several Debye lengths ($r_d = 2.1$ Å at the simulated concentration). For further details see the discussion of the charge densities below.

### 3.2. Orientation of water molecules

Fig. 4 shows the orientational distribution of the water dipole moment in the adsorbate layer for each of the three simulations. The distributions are rather wide, even for the sizable positive and negative surface charges employed. The width of the distributions clearly rules out models that describe adsorbate water as an oriented water layer. The distribution at the potential of zero charge is similar to that of pure water using the same model.

There are only small differences between the distribution $p(\cos \vartheta)$ at the potential of zero charge and for the positively charged surface. Obviously, the substantial amount of $Cl^-$ inside the adsorbate water layer at the positive surface charge does not change the orientational distribution significantly. Orienting influences due to the electric field and due to the hydration of contact-adsorbed anions compensate each other. The chloride ions apparently screen the positive surface charge to a large extent so that the water molecules experience similar average electric fields as near the uncharged surface.

However, when the surface is charged negatively, water molecules reorient and the maximum of the distribution changes from a set of orientations where the hydrogen atoms preferentially point into the solution to a preference of orientations where the hydrogen atoms point towards the surface. At the same time, the distribution becomes slightly narrower, since the orienting influences of electric field and hydration act in the same direction and tend to align water molecules. The behavior can be regarded as the partial ordering of water dipoles in the electric field of a 'capacitor' consisting of the surface charge and the $Na^+$ charge between first and second layer.

### 3.3. Charge densities

From the behavior of the orientation distribution functions of interfacial water molecules, it becomes clear that the solvent contributes substantially to the electrostatic behavior of the liquid near the interface. Because of its dipolar nature, the solvent cannot screen the surface charge. However, as will become apparent below, the solvent is able to compensate local excesses of free charges to some extent. It is therefore illustrative to investigate the charge densities of free (ionic) and bound (water) charges separately.

Fig. 5 shows, from top to bottom, the ionic charge densities for the positively, neutral and negatively charged metal surface. The data have been boxed to integrate out statistical noise. The bars at $z = 0$ for the two charged surfaces represent the surface charge of the electrode. The density of free charges decays rapidly with increasing distance from the electrode. The interface with the uncharged surface exhibits a small dipole of ionic origin, with predominantly positive charges in the region 2.5 Å $< z <$ 5 Å and predominantly negative charges in the region 5 Å $< z <$ 8 Å. The dipolar charge distribution is the consequence of the fact that the average position of $Na^+$ ions is closer to the uncharged surface than the average position of $Cl^-$ ions.

For both charged surfaces the surface charge is overscreened. The total amount of countercharge in the region 2 Å $< z <$ 3 Å (for the positively charged surface) and in the region 2.5 Å $< z <$ 5 Å (for the negatively charged surface) is larger in magnitude than the surface charge. For distances beyond 3 Å for the positively and 5 Å for the negatively charged surface, there is an excess of co-ions. Beyond about 10 Å, the free charge density is equal to zero within the limits of statistical uncertainty.

Fig. 6 displays the total charge density, which is the sum of the free charge density arising from the ion distribution and the bound charge density arising from the partial charges of the water model and the two components. All densities have been subjected to a Gaussian filter $w(z)$.

$$w(z) = \sqrt{\frac{2}{\pi\sigma^2}}\exp[-2(z/\sigma)^2]. \quad (5)$$

with half width $\sigma = 2.85$ Å, which is the diameter of a water molecule. The filtering process does not only smooth the data but also attempts to model the finite extent of the charge distribution in water molecule and ions, which, in reality, is not point-like as in the simulation models. A similar procedure has been justified by Wilson et al. [33] in their study of the surface potential of the liquid water/vapor interface. The total

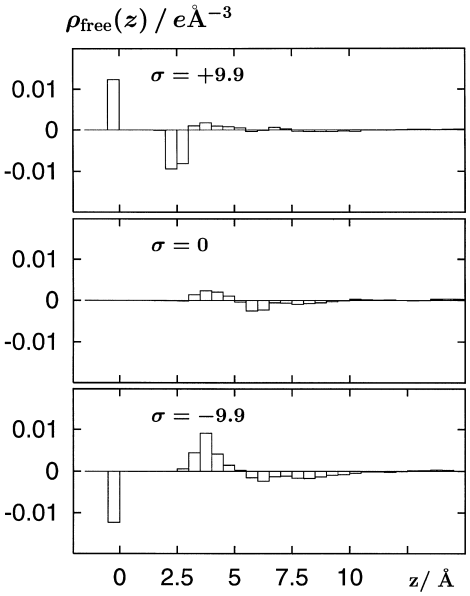


Fig. 5. Free (ionic) charge density profiles for three simulations with different surface charge densities as indicated.

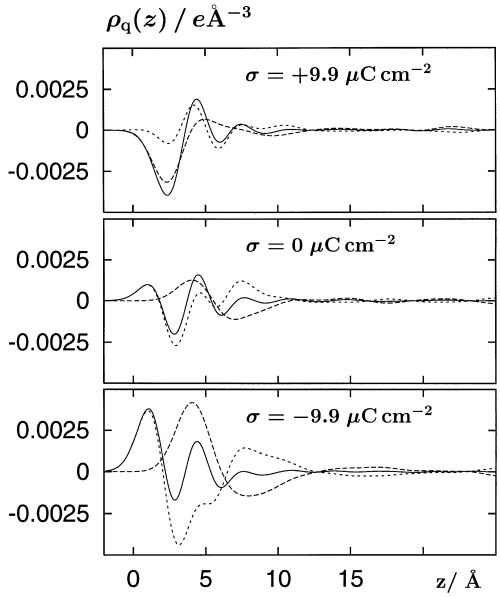


Fig. 6. Charge density profiles simulations with different surface charge densities as indicated. The charge density profiles are convoluted with a Gaussian of half width $\sigma = 2.85$ Å according to Eq. (5); full line: total charge density, long dashes: ionic charge density, short dashes: aqueous charge density.

charge density close to the interface is dominated by the water charges for $\sigma = 0$ μC cm$^{-2}$ and $\sigma = -9.9$ μC cm$^{-2}$ where the direct adsorption of ions is negligible. Only for the positive surface charge, $\sigma = +9.9$ μC cm$^{-2}$, where $Cl^-$ is adsorbed directly on the surface, the total charge density close to the electrode is dominated by the ionic charge density. Further away from the electrode, free and bound charges compensate each other to a large extent. The same effect has been noted previously by Glosli and Philpott [4, 11, 12].

### 3.4. Electric fields and interfacial potential

Figures 7 and 8 display the electric field, $E$, and the electrostatic potential, $\chi$, respectively, obtained by solving Poisson's equation in one dimension with the charge densities of Fig. 6 according to

$$E(z) = \frac{1}{\epsilon_0}\int_0^z q(z')\,\mathrm{d}z' \tag{6}$$

and

$$\chi(z) = -\int_0^z E(z')\,\mathrm{d}z' = -\frac{1}{\epsilon_0}\int_0^z q(z)\cdot(z-z')\,\mathrm{d}z' \tag{7}$$

The total electric field and the total electrostatic potential vary over a distance range of approximately 10 Å. The partial fields and potentials due to the free and the bound charges are different from zero on a somewhat larger length scale, but beyond about 10 Å the two contributions compensate entirely. Due to the large statistical noise present even in the long simulations discussed here, it cannot be ruled out that the ionic density distributions will become, with additional simulation time, more constant in this region, resulting in a decay of the component profiles on the same length scale as the total ones.

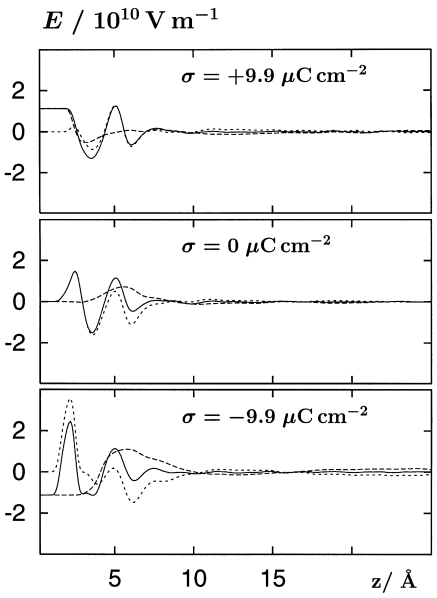


Fig. 7. Electric fields; full line: total charge density, long dashes: ionic charge density, short dashes: aqueous charge density.

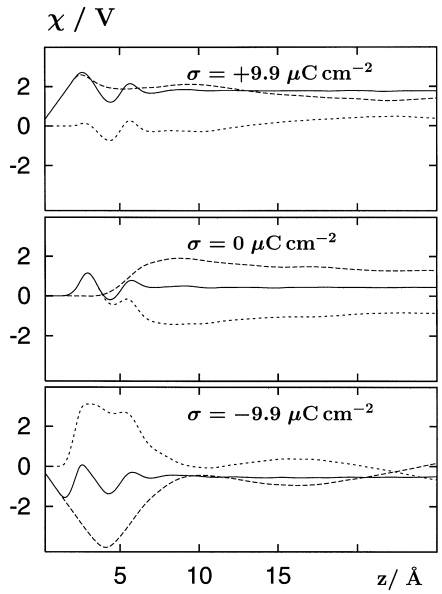


Fig. 8. Electrostatic potentials; full line: total charge density, long dashes: ionic charge density, short dashes: aqueous charge density.

We define the potential drop due to the liquid phase as the value of the electrostatic potential in the center of the bulk phase at $z = 20$ Å and obtain values of $\chi(20)$ of 1.79, 0.43 and –0.53 V for $\sigma = +9.9$, 0 and –9.9 μC cm$^{-2}$, respectively. The potential difference between $\sigma = +9.9$ μC cm$^{-2}$ and $\sigma = 0$ μC cm$^{-2}$ is slightly larger than that between $\sigma = 0$ μC cm$^{-2}$ and $\sigma = -9.9$ μC cm$^{-2}$, indicating an asymmetry of the potential–charge curve. The construction of a differential capacitance curve, however, would require many more simulations with significantly more precise values of $\chi(20)$, and is currently almost impossible with available computer resources.

## 4. Summary and discussion

The results of a series of simulations of aqueous NaCl solutions in contact with charged and uncharged metal surfaces have been presented. It is the first study in which the surface charge density of the model electrode is varied from negative through positive values. Very long simulations in excess of 2 ns are necessary in order to obtain reasonably converged ionic distri-

butions in the vicinity of the electrode. Even then, the high electrolyte concentration of 2.2 mol/l has to be chosen in order to be able to average over a sufficient number of ions.

One of the central goals of this study was the investigation of asymmetries in the electric double layer when sweeping the electrochemical potential from values corresponding to negative surface charge densities to those characteristic of positively charged surfaces. A very simplistic model, in which water molecules and ions interact with the metal atom cores by means of the same short range potential, and electrostatic effects are accounted for by the image charge model, was therefore chosen. This symmetric model allows us to focus on the difference between $Na^+$ and $Cl^-$ ions. No specific interactions are included. Nevertheless, there is clear evidence for characteristic differences between $Na^+$ and $Cl^-$. At all surface charge densities, the position of closest approach of the cation is between the first and second water layer. Only the height and thus the amount of ions in this layer increases when shifting the surface charge density from negative to positive values. The position of closest approach of the $Cl^-$ anion, on the other hand, changes with the surface charge of the electrode. $Cl^-$ ions are contact-adsorbed on positively charged electrodes. The equilibrium position of the first anion layer is shifted into and beyond the second water layer for negative surface charge densities.

The molecular model of the system does not include any specific interactions between anion and metal surface. Therefore, the different behavior of cations and anions must be entirely due to the differences in hydration. The hydration energy of $Na^+$ is, on the basis of the chosen model parameters, strong enough to prevent partial dehydration of the cation at negative surface charges. On the other hand, $Cl^-$ ions readily lose part of their hydration shell when the surface charge density is positive. This is consistent with recent computer simulations by Philpott and Glosli [4, 11, 12], who used a similar model with slightly different parameters and with the early interpretation of differential capacitance data of the mercury drop electrode by Grahame et al. (Refs. [34–39] and references therein). In their study, Philpott and Glosli investigated the concentration dependence of the electric double layer only at positive surface charge densities and noticed a concentration effect.

The asymmetry of the charge distribution gives rise to an asymmetry of the average electric field and the electrostatic potential at the interface. The simulations show that the electrostatic potential produced by the ionic charge density is compensated to a large degree by the potential arising from the water dipoles. At vanishing and negative surface charge densities, where no substantial direct adsorption is observed, the electrostatic field produced by the water molecules dominates the total effect. Thus, the simulations clearly demonstrate the importance of the solvent in a realistic description of the electrochemical interface.

The electrocapillary measurements of alkali halide solutions near the mercury electrode by Grahame [34–39] also show an asymmetry of the differential capacitance curves around the potential of zero charge. The data were interpreted in such a way that, with the exception of the fluoride ion, all halide ions are contact-adsorbed at surface charge densities slightly negative or slightly positive of the potential of zero charge. The present simulation study shows that, for a simple model, contact adsorption is possible even without specific interactions between ions and metal surfaces as a consequence only of the interplay between hydration and adsorption. Recently, in situ scanning tunneling microscopy and surface X-ray scattering studies proved that chloride, bromide and iodide form ordered monolayers on gold and platinum electrodes [40–46], indicating the presence of specific interactions between halide ions and transition metal surfaces. In a recently initiated study in our group, we will compare the predictions of the present model and of a model which includes specific adsorption of chloride ions and thus assess the importance of specific interactions [47].

The model presented here has several limitations. The first is, that the surface charge density can only be varied in integer multiples of the electronic charge divided by the surface area of the simulation cell. The latter is rather small in the present study, resulting in a smallest possible increment for the surface charge density of 4.95 $\mu C\ cm^{-2}$. In order to be able to resolve an experimental capacitance curve, the interface area needs to be increased, which in turn means that the number of particle in the simulation needs to be increased. This larger system should also be simulated for a longer real time in order to reduce the statistical uncertainties of the electrostatic potential calculation. The cost of such simulations is, at present, forbidding. Second, while the electrolyte phase is described by a realistic molecular model, the metal phase is not. Specific interactions and partial charge transfer are not accounted for. Since the electronic response to the electrolyte solution is not included in the model, the important contribution of the metal to the interfacial potential cannot be calculated. We note here that Schmickler and Leiva [48] and Shelley et al. [49] have made first calculations to use the jellium model to calculate the metal contribution to the capacitance. Their studies, however, were limited to pure water in contact with an electrode. A final limitation of the present study is the high concentration necessary to obtain a reasonable statistical accuracy. It is in principle possible to approach the limit of infinite dilution by calculating the potential of mean force, i.e. the variation of

the free energy of a single ion with distance from the surface and calculations of the kind have been performed by various authors [22, 50–56]. However, the single ion calculations do not allow simple control over the surface charge density.

In summary, the studies for NaCl solutions yield a detailed molecular picture of the electrolyte side of the electrochemical double layer. The main result is the clear indication of the asymmetry of the double layer, produced by the balance between ion adsorption and hydration energies. Investigations of other electrolyte solutions, which are presently under way in our group, are expected to provide further insight into the double layer structure.

## Acknowledgements

Financial support by the Fonds der Chemischen Industrie is gratefully acknowledged.

## References

[1] K. Heinzinger, in: J. Lipkowski, P.N. Ross (Eds.), Structure of Electrified Interfaces, Frontiers of Electrochemistry, VCH, New York, 1993, ch. 7, p. 239.
[2] E. Spohr, Computer Modeling of Aqueous/Metallic Interfaces, Habilitationsschrift, Ulm, 1995.
[3] I. Benjamin, Chem. Rev. 96 (1996) 1449.
[4] M.R. Philpott, J.N. Glosli, in: G. Jerkiewicz, M.P. Soriaga, K. Uosaki, A. Wieckowski (Eds.), Solid–Liquid Electrochemical Interfaces, ACS Symposium Series, vol. 656, ACS, Washington, 1997, ch. 2, pp. 13–30.
[5] E. Spohr, in: G. Jerkiewicz, M.P. Soriaga, K. Uosaki, A. Wieckowski (Eds.), Solid–Liquid Electrochemical Interfaces, ACS Symposium Series, vol. 656, ACS, Washington, 1997, ch. 3, pp. 31–44.
[6] H.L.F. von Helmholtz, Ann. Physik 89 (1853) 211.
[7] G. Gouy, J. Phys. 9 (1910) 457.
[8] D.L. Chapman, Philos. Mag. 25 (1913) 475.
[9] O. Stern, Z. Electrochem. 30 (1924) 508.
[10] R. Parsons, in: J.O. Bockris, B.E. Conway (Eds.), Modern Aspects of Electrochemistry, vol. 1, Academic Press, New York, 1954.
[11] M.R. Philpott, J.N. Glosli, J. Electrochem. Soc. 142 (1995) L25.
[12] M.R. Philpott, J.N. Glosli, S.B. Zhu, Surf. Sci. 335 (1995) 422.
[13] E. Spohr, K. Heinzinger, J. Chem. Phys. 84 (1986) 2304.
[14] K. Heinzinger, Mol. Sim. 16 (1996) 19.
[15] K. Heinzinger, in: M. Doyama, J. Kihara, R. Yamamoto (Eds.), Computer Aided Innovation Of New Materials II, Elsevier, Amsterdam, 1993.
[16] J. Seitz-Beywl, M. Poxleitner, K. Heinzinger, Z. Naturforsch. 46a (1991) 876.
[17] H.J.C. Berendsen, J.R. Grigera, T.P. Straatsma, J. Phys. Chem. 91 (1987) 6269.
[18] P. Bopp, W. Dietz, K. Heinzinger, Z. Naturforsch. 34a (1979) 1424.
[19] D.E. Smith, L.X. Dang, J. Chem. Phys. 100 (1994) 3757.
[20] L.X. Dang, Chem. Phys. Lett. 200 (1992) 21.
[21] S.H. Lee, J.C. Rasaiah, J. Chem. Phys. 101 (1994) 6964.
[22] E. Spohr, J. Mol. Liquids 64 (1995) 91.
[23] P.A. Thiel, T.E. Madey, Surf. Sci. Rep. 7 (1987) 211.
[24] S.E. Feller, R.W. Pastor, A. Rojnuckarin, S. Bogusz, B.R. Brooks, J. Phys. Chem. 100 (1996) 17011.
[25] J.C. Shelley, G.N. Patey, Mol. Phys. 88 (1996) 385.
[26] E. Spohr, J. Chem. Phys. 107 (1997) 6342.
[27] M.P. Allen, D.J. Tildesley, Computer Simulations of Liquids, Oxford University Press, New York, 1987.
[28] H.J.C. Berendsen, J.P.M. Postma, W.F. van Gunsteren, A. DiNola, J.R. Haak, J. Chem. Phys. 81 (1984) 3684.
[29] M.A. Wilson, A. Pohorille, L.R. Pratt, Chem. Phys. 129 (1989) 209.
[30] I. Benjamin, J. Chem. Phys. 95 (1991) 3698.
[31] M.A. Wilson, A. Pohorille, J. Chem. Phys. 95 (1991) 6005.
[32] J.O. Bockris, A.K.N. Reddy, Modern Electrochemistry, vol. 2, Plenum Press, New York, 1977.
[33] M.A. Wilson, A. Pohorille, L.R. Pratt, J. Chem. Phys. 99 (1988) 3281.
[34] D.C. Grahame, Chem. Rev. 41 (1947) 441.
[35] D.C. Grahame, R.P. Larsen, M.A. Poth, J. Am. Chem. Soc. 71 (1949) 2978.
[36] D.C. Grahame, E.M. Coffin, J.I. Cummings, M.A. Poth, J. Am. Chem. Soc. 74 (1952) 1207.
[37] D.C. Grahame, J. Am. Chem. Soc. 76 (1954) 4819.
[38] D.C. Grahame, B.A. Soderberg, J. Chem. Phys. 22 (1954) 449.
[39] D.C. Grahame, J. Am. Chem. Soc. 79 (1957) 2093.
[40] S.-L. Yau, C.M. Vitus, B.C. Schardt, J. Am. Chem. Soc. 112 (1990) 3677.
[41] R. Vogel, H. Baltruschat, Surf. Sci. 259 (1991) L739.
[42] X.J. Gao, M.J. Weaver, J. Am. Chem. Soc. 114 (1992) 8544.
[43] W. Haiss, J.K. Sass, X.J. Gao, M.J. Weaver, Surf. Sci. 274 (1992) L593.
[44] N.J. Tao, S.M. Lindsay, J. Phys. Chem. 96 (1992) 5213.
[45] B.M. Ocko, G.M. Watson, J. Wang, J. Phys. Chem. 98 (1994) 897.
[46] O.M. Magnussen, B.M. Ocko, R.R. Adzic, J.X. Wang, Phys. Rev. B 51 (1995) 5510.
[47] A. Kohlmeyer, E. Spohr, in preparation.
[48] W. Schmickler, E. Leiva, Mol. Phys. 86 (1995) 737.
[49] J.C. Shelley, G.N. Patey, D.R. Bérard, G.M. Torrie, J. Chem. Phys. 107 (1997) 2122.
[50] D.A. Rose, I. Benjamin, J. Chem. Phys. 95 (1991) 6956.
[51] E. Spohr, Chem. Phys. Lett. 207 (1993) 214.
[52] L. Perera, M.L. Berkowitz, J. Phys. Chem. 97 (1993) 13803.
[53] D.A. Rose, I. Benjamin, J. Chem. Phys. 98 (1993) 2283.
[54] D.A. Rose, I. Benjamin, J. Chem. Phys. 100 (1994) 3545.
[55] E. Spohr, Acta Chem. Scand. 49 (1995) 189.
[56] B. Eck, E. Spohr, Electrochim. Acta 42 (1997) 2779.